Complementary Colloid and Collector Nanoscale Heterogeneity Explains Microparticle Retention Under Unfavorable Conditions

Journal:	*Environmental Science: Nano*
Manuscript ID	EN-ART-08-2020-000815.R2
Article Type:	Paper

Environmental Significance Statement

Nanoscale heterogeneity governs the retention of nano- and micro-particles in environmental granular media such as saturated sands and gravels that are important groundwater resources. Constraining the sizes and prevalence of nanoscale heterogeneity on surfaces is critical to predicting particle transport in contexts spanning water resource protection from pathogens to remediation of groundwater *via* targeted delivery of reactive agents. By incorporating discrete representative nanoscale heterogeneity on simulated surfaces, we constrained by comparison of simulations to experimental observations the scales and prevalence of nanoscale heterogeneity relevant to particle transport and retention in environmental granular media.

Complementary Colloid and Collector Nanoscale Heterogeneity Explains Microparticle Retention Under Unfavorable Conditions

Cesar A. Ron[1], William P. Johnson[1,*]

[1]Department of Geology & Geophysics, University of Utah, Salt Lake City, UT 84112, USA

*Corresponding author. Email: william.johnson@utah.edu. Tel.: +1 801 585 5033

Abstract

Nano- and micro-scale particle (colloid) retention in environmental granular media is greatly reduced when the profile of colloid-grain surface interactions as a function of their separation distance includes a repulsive barrier. Under such unfavorable attachment conditions, typical of environmental settings, simulation of colloid retention predicts zero retention unless nanoscale heterogeneity is included to locally reduce or eliminate the repulsive barrier and allow attachment to the grain (collector). Simulations previously incorporated nanoscale heterogeneity on either the collector or the colloid, whereas complementary contributions of collector and colloid nanoscale heterogeneity have not been previously examined to the knowledge of the authors. The sizes and surface coverages of nanoscale heterogeneity on colloid (carboxylate modified polystyrene latex, CML) and collector (silica) surfaces that act complementarily to explain experimentally-observed retention in impinging jet experiments was herein examined for colloid sizes ranging from 0.11 to 6.8 μm at pH ranging 6.7 to 8.0 and ionic strength (IS) ranging 6.0 to 20.0 mM. We demonstrate that complementary contributions of power law size-distributed nanoscale heterogeneity; 25 to 90 nm radii on the collector; 5 to 60 nm radii on the colloids, captured the observed retention across the entire colloid size range (including previously uncaptured retention of > 2.0 μm CML) for all pH and IS conditions. This approach greatly reduced the required maximum size of heterodomains (nanoscale attractive zones) from 320 nm radii required when heterogeneity was incorporated solely on either the collector or colloid surface and constrains the scales of spectroscopically-observed surface heterogeneity relevant to colloid retention.

Introduction

Predicting the retention of nano- and micro-particles in environmental granular porous media underlies protection of groundwater resources from pathogens including nanoscale viruses (*e.g., rotavirus*) and microscale protozoa (*e.g.*, c*ryptosporidium parvum*)[1–4] and subsurface remediation *via* targeted delivery of engineered colloids ranging from nanoscale zero-valent iron to microscale biochar.[5–11] We herein refer to nano- and micro-particles as colloids for ease of reference. At the pore scale, colloid retention involves mass transport from bulk fluid to

grain surfaces, and subsequent attachment.[12,13] Retention is quantified as collector efficiency, η, which is the fraction of colloids that are retained relative to those that enter the collector (representative grain plus fluid shell).

Attachment is moderated by colloid-collector interactions arising from physicochemical characteristics of their surfaces as moderated by properties of the fluid.[14] Some interactions can be attractive (*e.g.*, van der Waals interactions for positive combined Hamaker constants) while others can be repulsive (*e.g.*, electric double layer interactions for like-charged surfaces).[14–16] Because the various colloid-collector interactions decay at different rates as a function of separation distance, repulsive interactions such as electric double layer (EDL) may dominate at intermediate separation distances between a few nm and several tens of nm, generating a repulsive barrier, and so-called unfavorable conditions for attachment.[17–23] Calculated forces and torques under unfavorable conditions predict no attachment when the repulsive energy barrier exceeds approximately 10kT. Energy barrier magnitudes calculated from measured ζ-potentials of environmental surfaces are typically orders of magnitude larger than this threshold.[17] However, colloid attachment under unfavorable conditions is routinely observed in environmental granular media.[17]

At the continuum scale, for each collector passed, retention of a fraction of the colloid population (as quantified by η) yields compounded loss, such that colloid concentration is expected to decrease exponentially with increasing transport distance (*e.g.*, Li et al.,[24] Johnson and Hilpert[25]). However, this exponential decrease is observed only under favorable conditions,[24,25] whereas observed colloid distributions from source are non-exponential under unfavorable conditions, even for monodisperse colloids, in both field[26–31] and laboratory[24,25,32,33] settings. This profound transition from exponential to non-exponential colloid distribution from source accompanying the transition from favorable to unfavorable conditions is the primary characteristic that underlies our investigation.

Whereas dynamic flow, grain shape, and grain size distributions are additional critically important attributes of environmental granular media, we examine steady-state flow and granular media comprised by uniform spherical grains in order to examine the impact of

favorable versus unfavorable conditions. Our experimental pore-scale system represents the forward flow stagnation zone on porous media grains, which are well-known *loci* of colloid delivery to grain surfaces.[12] Such pore-scale single-focal plane observations of colloid retention and re-entrainment inform mechanistic simulations, which when upscaled with additional assumptions regarding network-scale transport, reproduce the observed non-exponential colloid distributions from source.[34,35]

To predict attachment under unfavorable conditions lacking macroscale heterogeneity, nanoscale heterogeneity (local zones of nanoscale attraction) must be represented on the bulk repulsive surface.[22,23,30,36–41] Current analytical techniques (*e.g.*, X-ray photoelectron spectroscopy, atomic force microscopy) can detect nanoscale heterogeneity,[21,42–44] however, the significance of detected scales and surface coverages to colloid retention is unclear. To constrain scales and surface coverages of nanoscale heterogeneity relevant to colloid retention, discrete representative nanoscale heterogeneity (DRNH) was developed for prediction of colloid retention on overall repulsive surfaces.[22,23,41] The basis for DRNH is that as colloids move into proximity with heterodomains (nanoscale zones of opposite charge to bulk surface), colloid-collector interactions will be net repulsive or net attractive depending on the fraction of the zone of interaction (ZOI) occupied by heterodomain(s)[39] (Figure 1a). Because the ZOI increases with colloid size and contracts with increased ionic strength (IS),[39] colloid-collector interactions depend on colloid size and solution IS, thus allowing DRNH to be obtained *via* comparison of colloid trajectory simulations to experiments under varied colloid size, fluid velocities, IS, and pH values.[22,23,41]

Upon reaching the near-surface fluid domain *via* mass transport (diffusion, settling, and fluid drag), simulated colloids experience repulsion and translate across the collector surface until they encounter a condition wherein the fraction of ZOI area occupied by heterodomains (AF) is sufficient to reduce or eliminate the repulsive barrier and allow attachment. The likelihood of meeting this condition increases with the likelihood of encountering heterodomains on the collector (HETC), which increases with increased diffusion and fluid drag in the near-surface pore water.[41] The likelihood of encountering heterodomains also increases with increasing

surface coverage (SCOVC) and size (R_{HETC}) of HETC until HETC become sufficiently large and prevalent to guarantee attachment (AF > threshold) regardless of colloid location.

In previous approaches[22,23,41], DRNH was assumed to follow a power-law size distribution under the reasonable assumption that larger heterodomains reflect natural clustering (*via* random location) of smaller heterodomains, such that spatial frequencies of heterodomains (or heterodomain clusters) decrease with increasing size. DRNH comprising a power law distribution of heterodomains on the collector surface (Figure 1b, closed circles), explained the observed minimum η in the size range corresponding to the n-μ transition (0.2 to 2.0 μm diameter) for carboxylate-modified latex colloid (CML) retention on silica[41] (Figure 2, red dotted lines versus triangles). However, these colloid trajectory simulations, which incorporated DRNH solely on the collector, significantly under-predicted experimentally-observed η under unfavorable conditions for CML of sizes exceeding 2.0 μm (Figure 2, red dotted lines versus triangles). In order to match the observed η values, DRNH surface coverages for the largest heterodomains (capturing the largest colloids) would necessarily violate a power law distribution, wherein per area and fractional surface coverages of the largest heterodomains would exceed those of smaller heterodomains (Figure 1a, open versus closed circles and SI, Figure SI-1). This discrepancy, and the observation that > 2.0 μm colloids of various compositions (biological and non-biological) show near-favorable η under unfavorable conditions,[41] suggest that heterodomains on the colloid surface may increase retention of these larger colloids.

Previous simulations have accounted for nanoscale heterogeneity as nanoscale zones of opposite charge to bulk surface (heterodomains) on either the collector[22,23,39,41,45] or the colloid,[46–48] or both.[49] Comparison of the kinetics of attachment *via* either heterodomains on colloid or collector[46] demonstrates that the attachment process is at least 50% slower *via* colloid heterodomains if fractional surface coverage by heterodomains is sufficiently low that colloid rotation becomes a factor in the likelihood of their projection falling within the colloid-collector ZOI. To the knowledge of the authors no study has examined the complementary impact of heterogeneity on both the collector and colloid surfaces for the purpose of

constraining heterodomain sizes that explain experimental results. Therefore, our objective is to explore the conditions under which heterodomains on the collector and the colloid (HETC and HETP, respectively) produce colloid attachment through complementary contributions of attractive interactions within the ZOI. The central hypothesis of this study is that complementary contributions from power law-distributed HETC and HETP may produce the experimentally-observed η of > 2.0 μm colloids while preserving the match of simulated to observed colloid retention for smaller colloids, and while reducing the maximum heterodomain sizes necessary to explain colloid retention. We test this hypothesis *via* mechanistic colloid trajectory simulations incorporating DRNH on both collector and colloid surfaces, under conditions that allow implicit representation of colloid rotation.

Methods

Experiments examined retention of carboxylate-modified polystyrene latex (CML) fluorescent microspheres (λ_{ex} = 505, λ_{em} = 515 nm) (Molecular Probes Inc., Eugene, OR) of six diameters (0.11, 0.25, 1.1, 2.0, 4.4 and 6.8 μm) on soda-lime glass slides and coverslips (herein referred to silica) (Fisher Scientific, Inc.) in and impinging jet flow cell, as previously reported in Ron et al.[41]

Colloidal suspensions

Colloid suspensions were prepared from stock in relevant solution with concentrations ranging from 2.5E5 to 2.5E7 microspheres per mL. The microsphere suspension concentration was determined *via* vacuum filtration of colloid solution (volume adjusted to ensure > 20 CML per observation area) on 0.05 or 0.1 μm polycarbonate filters (Millipore) followed by averaging counts of 45 random observation areas using wide-field fluorescence for colloid illumination and scaling this average to the area of deposition on the filter. The relative standard deviation of counts was 10% or less demonstrating uniform colloid deposition across the filter.

Suspension ionic strength (IS) was adjusted using NaCl. Unfavorable solutions (6.0 mM and 20.0 mM IS) were buffered with 2.2 mM MOPS (3-Morpholinopropane-1-sulfonic acid) (Sigma-Aldrich Corp.) with pH set to 6.7 and 8.0 using NaOH (0.5 M). The ion contribution from the buffer was accounted for when calculating the solution ionic strength. Favorable solutions

were achieved by increasing the solution ionic strength to 50.0 mM and decreasing the pH to 2.0 using HCl (1.3 M). In cases where ζ-potentials of the collector and colloid were both slightly negative, the net interaction was attractive.[50]

CML electrophoretic mobility (EPM) was measured in suspensions using ζ-potential analyzer (Mobiuζ, Wyatt Technology Corp., Santa Barbara, CA). CML ζ-potentials were calculated from EPM *via* the Smoluchowski equation[51] (SI, Table SI-1). CML roughness was measured with an atomic force microscope (model N9451A Agilent Technologies; Santa Clara, CA). CML RMS roughness was 13.0 ± 7.0 nm (1.1 μm), 10.0 ± 7.0 nm (2.0 μm), 13.0 ± 6.0 nm (4.4 μm), and 27.0 ± 9.0 (6.8 μm).[40]

Collector surface

Silica slides were cleaned *via* the SC-1 procedure[52] prior to every experiment. Silica ζ-potentials were adopted from representative values reported in the literature[53,54] (SI, Table SI-2). Silica RMS roughness was 1.0 ± 0.7 nm as measured with an atomic force microscope (model N9451A Agilent Technologies; Santa Clara, CA).[40]

Impinging jet experiments

A custom-made stainless-steel impinging jet flow cell (radially symmetric) (SI, Figure SI-2) was used to observe colloid attachment and detachment, as described in previous studies.[22,23,50] The jet (cell inlet) was 0.5 mm in radius, and the impinging surface was located 1.25 mm from the jet, perpendicular to the jet axis. To ensure an evenly radial distribution of the flow across the cell, four outlets were evenly spaced in a circular array at a radial distance 10.0 mm from the jet axis.

Colloid attachment experiments were conducted by injecting colloidal suspensions in the flow cell after 30 min of equilibration of the collector surface with injected colloid-free solution. Attachment was quantified as collector efficiency (η = number attached/number injected).[22,50] Experiments examined the following conditions: pH 6.7 and 8.0, 6.0 mM and 20.0 mM IS, and average jet velocity (v_{jet}) of 1.7E-3 ms^{-1} (or 2.2 $mday^{-1}$ average pore water velocity, and within the ranges relevant to environmental granular media[55,56]). The duration of the experiments

ranged from 1 to 6 h depending on rate of attachment. Colloids were illuminated using wide field fluorescence with a band-pass filter for excitation (478-493 nm) and a (405/488/543 nm) dichroic filter for emission (Chroma Technology Corp., Bellows Falls, VT). The 1.1 μm and larger CML were experimentally-observed using a 10x objective (Nikon, Japan), the 0.25 μm and smaller CML were observed using a 60X objective (Plan Apo TIRF DIC H; Nikon, Japan). The number of attached colloids at several time intervals (*e.g.*, 15 s) was tracked with images taken *via* a CoolSNAP HQ CCD camera (Photometrics, Tucson, AZ) and processed using image analysis software (MetaMorph, Universal Imaging Corp., Downingtown, PA). A detailed description of the optical setup is provided in previous publications studies.[22,23,50]

Colloid trajectory model

A Lagrangian colloid trajectory model developed for the impinging jet system (*e.g.*, Pazmino et al.[22]) was used to simulate CML trajectories. The model predicts delivery to the surface and attachment if the arresting torque exceeds the driving torque when the colloid is in contact with the surface. Simulated colloid trajectories are generated in response to Lagrangian integration of forces and torques acting on colloids; *i.e.*, fluid drag, colloid-collector surface interactions (XDLVO), lift, Brownian diffusion, virtual mass, and gravity, as described in previous publications.[22,50,57,58] Colloid-collector surface interaction forces include van der Waals (vdW), electric double layer (EDL), and Born interactions as described in previous publications,[22,50,57] whereas Lewis acid-base, steric forces, and roughness impacts, were more recently incorporated.[40,58] Hydration and other potential contributions to steric interactions were accounted for quantitatively using the approach of VanNess et al.[58] Nanoscale surface roughness has been shown to affect colloid-surface interactions.[59,60] For this reason, a modification of colloid-surface interactions was included for CML and collector surfaces, following the characterization described in Rasmuson et al.[40] The silica collector surface was considered smooth, since its RMS roughness was < 1.0 nm.[40] For CML, the RMS roughness used in simulations and slip layer effects were estimated as in Rasmuson et al.[40] (SI, Table SI-3).

Discrete Representative Nanoscale Heterogeneity (DRNH)

Simulations regarding colloid attachment under unfavorable conditions were performed by incorporating DRNH on the colloid and the collector surface. On the collector surface, HETC were "placed" at intervals in polar coordinate space (r and θ) from the impinging jet axis to generate uniformly spaced DRNH over the collector surface, as described and demonstrated in Pazmino et al.[22]

HETC were placed following a power-law distribution. This discrete representation of HETC sizes intends to approximate the expected continuous size distribution resulting from random clustering of nanoscale physical and chemical features.[39,45,46,61] On the colloid surface, HETP were "placed" at intervals in spherical coordinate space (r, ϕ, and θ) from the colloid axis to generate uniformly spaced DRNH over the colloid surface. To determine the contribution (constructive of destructive, Figure 3) to colloid-collector surface interactions, HETP partially of fully encompassed by the ZOI were projected onto the collector surface (Supporting Information). The projection of a HETP corresponds to an ellipse, unless the colloid z-axis passed through the heterodomain center, in which case the projection corresponds to a circle (SI, Figures SI-3 to SI-9). To reduce mathematical complexity ellipsoidal projected HETP were approximated as circles of equivalent surface area, with the largest discrepancy of the approximation being 1.3% (SI, Figure SI-10).

The linear superposition approximation (LSA) technique was used to calculate colloid-collector surface interactions. For the colloid size range analyzed in this study, the influence of the curvature of the colloid and collector surfaces within the ZOI is negligible.[20] Net colloid-collector interaction can therefore be determined by the sum of attractive and repulsive contributions without regard to their specific locations within the ZOI.[22,39]

For simplicity, heterodomain ζ-potentials were assumed to be of the same magnitude and opposite charge relative to the bulk surface of colloid and collector. This simplification is reasonable given that once the fractional coverage of ZOI by heterodomains is sufficient to eliminate the repulsive barrier to attachment, the attractive interaction, as indicated by collector efficiency, is relatively insensitive to the magnitude of the attractive ζ-potential as demonstrated in Pazmino et al.[22]

Results and Discussion

Limits on Surface Coverage and Size of Heterodomains

Our goal in comparing mechanistic trajectory simulations to experimentally-observed colloid retention is to constrain the sizes and surface coverages of heterodomains that govern colloid transport in granular media. Because colloid trajectory simulations under unfavorable conditions are computationally intensive even when colloid orientation (rotation) is implicit, we sought to determine the conditions under which explicit colloid rotation can be neglected without impacting the analysis. This involved determining the values of surface coverage (SCOVP) and radii (R_{HETP}) of HETP (heterodomains on the colloid) for which the fraction of ZOI occupied by attractive interactions was constant regardless of colloid orientation.

By numerically rotating colloids with uniformly spaced HETP across 100 uniform increments of a full rotation around each of three orthogonal axes (1E6 increments total) (SI, Figure SI-11), the threshold SCOVP for a given R_{HETP} was determined that guaranteed the ZOI would encompass at least one HETP regardless of colloid orientation. These threshold SCOVP values increased rapidly with increased R_{HETP} for all colloid sizes (Figures 1c and SI, Figure SI-12a). The threshold SCOVP that guarantees the presence of at least one HETP within the ZOI does not guarantee that AF is sufficient to eliminate the repulsive barrier.

The value of SCOVP for a given R_{HETP} at which the repulsive barrier was eliminated by sufficient HETP within the ZOI was determined by summing the repulsive and attractive XDLVO contributions within the ZOI. The threshold SCOVP corresponding to R_{HETP} that eliminated the repulsive barrier ranged from 0.35 to 0.55 across the range of RHETP examined and increased modestly with increased R_{HETP} (Figures 1c and SI, Figure SI-12b).

The intersection of the two above-described limits defines a space within which combinations of SCOVP and R_{HETP} allow meaningful transport simulations without explicit colloid rotation (Figure 1c). In the space above the dashed lines (Figure 1c), all simulations yield favorable colloid retention. In the space to the right of the solid lines (Figure 1c), explicit colloid rotation is required since the existence of at least one HETP within the ZOI is not guaranteed regardless

of colloid orientation. The SCOVP versus R_{HETP} space corresponding to a larger range of SCOVP is provided in SI, Figure SI-12.

The above analysis concerns solely heterodomains on the colloid (HETP). However, different collector surfaces yield different retention for the same colloid under equivalent conditions,[23] demonstrating that heterogeneity on the collector (HETC) is at least partially responsible for observed colloid retention. Complementary contributions by HETC and HETP to AF define the requisite R_{HETC} and R_{HETP} required to eliminate the repulsive barrier under the limiting condition where HETC exists fully within the ZOI without overlapping with the projection of HETP (Figure 3a), such that their contributions to AF are solely constructive. This limiting condition (non-overlapped pair) contrasts with overlapping projected HETC and HETP in the ZOI which generates destructive (repulsive) interaction (Figure 3b).

Under the above limiting condition of monogamous non-overlapped HETC and HETP (solely constructive), Equation 1 determines the requisite R_{HETC} and R_{HETP} as shown by the quarter circle lines (Figure 4), which have greater size for larger colloids due to their larger ZOI under a given IS, as well as greater size for a given colloid size under lower IS (Figure 4a versus b) due to ZOI expansion with decreased IS.

$$\mathrm{AF} = \left(\mathrm{R}_{\mathrm{HETC}}^2 + \mathrm{R}_{\mathrm{HETP}}^2\right) \Big/ \mathrm{R}_{\mathrm{ZOI}}^2 \qquad (1)$$

The areas interior to the quarter circles (Figure 4) correspond to R_{HETC} and R_{HETP} that may eliminate the repulsive barrier only if multiple HETC or HETP exist partially or fully within the ZOI. For each colloid size there is a threshold R_{HETP} above which HETP are too few in number to guarantee that one HETP will lie within the ZOI regardless of colloid orientation. The dashed portions of the quarter circle lines (Figure 4) indicate this condition. For HETC in the absence of HETP, and vice versa requisite heterodomain radii under the limiting condition are approximately: 21, 31, 66, 88, 131 and 154 nm for 0.11, 0.25, 1.1, 2.0, 4.4, and 6.8 μm colloids, respectively, under the 6 mM IS and pH 8.0 condition, and are decreased with increased IS (Figure 4 x- and y- axes, respectively). While the above exploration of solely constructive interactions illustrates requisite complementary heterodomain sizes, trajectory simulations

accounted for all possible contributions (both constructive and destructive), as described below.

Colloid Retention (η) from Trajectory Simulations

To explore our hypothesis that complementary contributions from heterodomains on collector (HETC) and colloid (HETP) surfaces explain experimentally-observed η values for > 2.0 μm CML, colloid trajectories were simulated in an impinging jet system (*e.g.*, Pazmino et al.[22]). The simulations concerned unfavorable attachment conditions with incorporation of DRNH on both the collector and colloid surfaces under the surface coverage and size limits described above. The values of SCOVC, R_{HETC}, SCOVP and R_{HETP} were varied within the limits described above, and while imposing a power law inverse relationship between their size and spatial frequency (Figure 5a and b), to determine whether complimentary contributions from heterodomains HETC and HETP could produce experimentally-observed η values for all colloid sizes across varied pH and IS conditions.

The mechanistic trajectory simulations demonstrated that incorporating HETC and HETP allowed capture of experimentally-observed η values across the range of colloid sizes across the range of solution IS and pH (Figure 2, red solid lines versus triangles). Simulated values of η for < 2.0 μm CML equaled observed values to within a factor of three, as was attained when simulations incorporated HETC only. A factor of three was considered sufficient match to experiments given previously demonstrated factor-of-three discrepancies in predictions even under favorable conditions.[56] Simulated values of η for > 2.0 μm CML matched experimentally-observed near-favorable values (Figure 2, red solid lines versus triangles) using R_{HETC} ranging up to 90 nm (Figure 5a and b), whereas this was not possible in the absence of HETP even when R_{HETC} ranged up to 360 nm[41] (Figure 2, red dotted lines versus triangles). Furthermore, incorporating HETP preserved the observed minimum η for n-μ transition colloids (0.2 to 2.0 μm diameter), and its exaggeration with increased pH and decreased IS (Figure 2), as previously reported.[41] Below we describe how DRNH on both the collector and colloid surfaces was distributed according to a power law and how these sources of heterogeneity acted complementarily.

Collector and Colloid Heterodomain Properties

Hydrodynamic and colloid-collector interaction impacts of nanoscale roughness are incorporated into our simulations according to Rasmuson et al.[40] The hydrodynamic impact yields a non-zero tangential velocity at the contact surface (tops of the asperities), wherein the slip layer terminates within the interior of the collector. Colloid-collector surface interactions scale with asperity sizes and the number of asperities within the ZOI. For asperity size yielding multiple points of contact, contact radii correspondingly increased, as demonstrated via direct observation of the impact of concavities when scales of roughness exceed colloid size.[62,63] This paper focuses on nanoscale heterogeneity in the form of surface charge because roughness alone cannot explain attachment[40] and observed sensitivity to IS indicates the predominance of charge heterogeneity in attachment. Thus, the impact of heterodomain size and surface coverage was determined independently while accounting for the impacts of roughness.

HETC were represented by three radii (R_{HETC}): 90, 45 and 25 nm with spatial frequency ratios of 1, 8, and 64, respectively (Figure 5a and b), and with all three sizes present on the simulated collector surface (SI, Figure SI-13). Because ZOI increases with increasing colloid size, a given R_{HETC} contributes significantly to repulsive barrier elimination for a limited range of colloid sizes. For pH values of both 6.7 and 8.0, as well as IS values of 6.0 and 20.0 mM, $R_{HETC} \geq 25$ nm captured 0.11 μm CML, $R_{HETC} \geq 45$ nm captured 0.11 and 0.25 μm CML, and $R_{HETC} \geq 90$ nm captured 0.11 to 2.0 μm CML. For R_{HETC} ranging 25 to 90 nm, capture of > 2.0 μm CML required complementary contributions from HETP.

HETP of a given size were uniformly distributed across the colloid surface, with R_{HETP} increasing with increasing colloid size (Figure 5c and d), under the assumption that smaller colloids do not accommodate larger HETP (SI, Figure SI-14), which is corroborated by random placement analysis described below. HETP were power law size distributed among the six colloid sizes, with HETP radii (R_{HETP}) being 5.0, 10.0, 15.0, 30.0, 47.7 and 57.5 nm for the 0.11, 0.25, 1.1, 2.0, 4.4, and 6.8 μm colloids, respectively (Figures 4 and 5c). SCOVP expressed as #heterodomains/μm^2 yielded a power law relationship (Figure 5c), whereas SCOVP expressed as fractional coverage exposed a step distribution (Figure 5d), wherein fractional coverage of

the largest HETP was a factor of 2 to 3 greater than fractional coverage of smaller HETP. This outcome is discussed further below.

The space within the boundaries set by the limiting condition (Figure 4) wherein multiple HETP or HETC may occupy the ZOI depending on SCOVP and SCOVC (Figure 1c), with constructive and destructive contributions (Figure 3), is further impacted by mass transport limitations which reduce the likelihood of encountering heterodomains. Mechanistic trajectory simulations accounted for these combined impacts, yielding values of R_{HETC} and R_{HETP} that explained experimentally-observed retention (Figure 4, closed circles). For > 2.0 μm colloid diameters, R_{HETC} and R_{HETP} predominantly fell within the quarter circle corresponding to the limiting condition (one non-overlapped pair) (Figure 4), whereas for ≤ 2.0 μm colloid diameters, R_{HETC} and R_{HETP} fell outside the quarter circle corresponding to this limiting condition (Figure 4).

Whether optimized R_{HETC} and R_{HETP} fell within or outside their quarter circle was governed by the combined and interrelated impacts of: i) transport limitations on encountering heterodomains; ii) multiple heterodomains within the ZOI; and iii) quantitative match to experimental η by reducing/increasing heterodomain prevalence according to the power-law size distribution. For > 2.0 μm colloid diameters, complementarity was required to capture experimentally-observed η, and so HETP dominated the attractive contributions to AF (Figure 1d, blue bars). For ≤ 2.0 μm colloid diameters, HETC was allowed to dominate attractive contributions to AF (Figure 1d, green bars), similarly to the condition where HETP were absent,[41] although it is likely that other R_{HETC} and R_{HETP} combinations can also explain the observed η for ≤ 2.0 μm CML. Representative final attachment configurations from mechanistic trajectory simulations involved complementary contributions from multiple HETP and one HETC, as shown in (Figure 6).

Under complimentary contributions from HETC and HETP, the size distribution of HETC followed a power law regardless of whether SCOVC was quantified as the number of heterodomains per area or fractional surface coverage by heterodomains (Figure 5a and b). In contrast to HETC, HETP approximated a power law size distribution (Figure 5c and d). When expressed as fractional surface coverage (Figure 5d), SCOVP was a factor of 2 to 3 greater for R_{HETP} > 40 nm

(CML > 2.0 μm) relative to R_{HETP} < 40 nm (CML ≤ 2.0 μm). In other words, explaining observed η for > 2.0 μm CML required increases in both R_{HETP} and SCOVP relative to smaller CML sizes. This is potentially explained by heterodomain clustering wherein random sequential non-overlapping placement of 10 nm heterodomains generated larger clusters on larger surface areas for a given surface coverage (SI, Figure SI-15). Natural clustering occurs for random location of moieties on surfaces (*e.g.*, defects, substitutions, and other heterogeneities) such that clusters are defined by neighboring moieties whose separation is less than a specified distance, and wherein smaller clusters greatly outnumber larger clusters (*e.g.*, power-law size distribution).[64–67] However, the increased SCOVP accompanying R_{HETP} for > 2.0 μm CML violates the expected power law decrease in frequency of HETP with increased R_{HETP} (SI, Figure SI-15). Whether this apparent result that larger colloids carry larger and more numerous HETP reflects a contrivance of our simulations or an actual attribute of microparticles remains to be determined in future work. Notably, Ron et al.[41] observed that > 2.0 μm colloids of various compositions (*i.e.*, biological and non-biological) had near-favorable η under unfavorable conditions, suggesting that they carry attributes distinct from smaller colloids that facilitate their near-unity attachment efficiencies.

Whereas SCOVC, R_{HETC}, SCOVP and R_{HETP} (Figure 5) were optimized using experimental data under 6.0 mM IS and pH 8.0 conditions, simulated η values emerged to be in good agreement with experimentally-observed η for the entire range of colloid size (0.11 to 6.8 μm) and under higher IS (20.0 mM) and lower pH (6.7). The influence of IS on experimentally-observed η values was captured in simulations (Figure 2) without changing SCOVC, R_{HETC}, SCOVP, or R_{HETP}; *i.e.*, that influence was accounted for by the impact of IS on the measured ζ-potentials (SI, Table SI-1), the calculated thickness of the electric double layer, and the calculated radius of the ZOI.

To capture the influence of pH, surface coverage by heterodomains on the collector (SCOVC) was decreased by an order of magnitude as pH increased from 6.7 to 8.0 (Figure 5a and b), consistent with the observed decreased ζ-potential with increased pH for silicate minerals and CML,[23] resulting from deprotonation of oxide moieties (silica) and carboxylic groups (CML). The

observed decrease in CML retention was well fit using an assumed decrease in frequency of protonated (positive) domains (heterodomains).[23] Likewise, surface coverage by heterodomains on the colloid (SCOVP) decreased by 4 to 20% in response to the pH increase from 6.7 to 8.0 (Figure 5c and d). That SCOVP was less sensitive to pH than was SCOVC reflects the different contributions to AF as a function of colloid size, wherein SCOVP dominated AF for > 2.0 μm colloids, and SCOVC dominated AF for ≤ 2.0 μm colloids (Figure 1d). The high SCOVP relative to SCOVC (two orders of magnitude for fractional surface coverage) that allowed implicit simulation of colloid rotation, made η more sensitive to changes in SCOVP relative to SCOVC, therefore requiring lesser sensitivity to pH in order to explain the experimental results.

SCOVP used herein cannot be compared to those operating in Shave et al.[46] for which the kinetics of attachment were demonstrated to be significant to due colloid rotation. This is because while Shave et al.,[46] reported mass of polymer per area of colloid and collector surfaces, they did not report heterodomain cluster sizes or surface coverages. However, their results suggest that if SCOVP were sufficiently low for colloid rotation to impact attachment in our experiments, our simulations would then need to increase SCOVC to allow SCOVP to decrease while allowing a simulated match to experimentally-observed η. The balance between SCOVC and SCOVP may be resolved with direct spectroscopic and spectrometric observations to further elucidate heterodomain cluster sizes and surface coverages.

The potential impact of assuming uniform placement of heterodomains deserves consideration. At the scale of the ZOI, heterodomain location and shape within the ZOI are inconsequential because the ZOI is nearly planar, such that separation distance and colloid-collector interaction change negligibly with location.[22] Therefore, non-uniform versus uniform placement of heterodomains within the ZOI is inconsequential. At the scale of the colloid, non-uniform distribution of heterodomains (*e.g.*, Janus colloid as an extreme example) would impact the surface coverages necessary to neglect explicit colloid rotation. Hence, our simulations that neglect colloid rotation may not represent colloids with highly non-uniform distributions of heterodomains. At the scale of the collector, non-uniform distribution of heterodomains may impact the value of η; hence, our simulations may not represent highly non-uniform

distribution of heterodomains on the collector. While non-uniform heterodomain coverage on colloids or collectors can be addressed with increased numerical intensity, our goal is to demonstrate impacts of complementary colloid and collector contributions assuming uniform distributions.

The influence of HETC and HETP ζ-potentials, which we assumed to be of equal magnitude and of opposite charge relative to their respective bulk surfaces, is weak with respect to retention (η), since at typical groundwater velocities retention is relatively insensitive to the depth of the primary minimum typically defined HETC and HETP ζ-potentials.[22,40] In contrast, the influence of HETC and HETP ζ-potentials is relatively strong with respect to detachment in response to fluid velocity and solution chemistry perturbations, since mobilization requires that the mobilizing torque exceed the resisting torque defined in part by the depth of the primary minimum.[22,40] Further refinement of heterodomain sizes and ζ-potentials will result from future comparison to detachment experiments, and by comparison to spectroscopic and other direct observations regarding heterogeneity in surface properties.

Significance

Our simulations incorporating DRNH on collector and colloid surfaces constrain the size range of nanoscale heterogeneity relevant to colloid attachment in granular media. Heterodomain sizes between 5 and 90 nm explain attachment of colloid sizes ranging between 0.11 and 6.8 μm. These size ranges serve as a guide for detection of nanoscale heterogeneity using surface analytical techniques such as X-ray photoelectron spectroscopy, atomic force microscopy, among others. By incorporating nanoscale heterogeneity on the colloid, we were able to better capture experimental observations while reducing the scale of nanoscale heterogeneity on the collector needed to simulate experimentally-observed retention. The simulations suggest that > 2.0 μm microparticles carry surface heterogeneity that facilitates their retention relative to smaller colloids. We expect our approach to be applicable to nanoparticles with Debye lengths not exceeding 10% of colloid size, *e.g.*, colloid sizes exceeding multiple tens of nm in diameter. Constraining nanoscale heterogeneity was performed using Fortran and MATLAB software that can also be utilized in design of heterogeneous collector and colloid surfaces for tuning desired

transport properties in biological and non-biological contexts, as well as for visualization in classroom and research contexts. This software is available at https://wpjohnsongroup.utah.edu.

Conflicts of interest

Authors declare no conflict of interest.

Acknowledgements

This article is based upon work supported by the National Science Foundation Program: Designing Materials to Revolutionize and Engineer our Future (DMREF) (1629078). Any opinions, findings, and conclusions or recommendations expressed in this material are those of the authors and do not necessarily reflect the views of the National Science Foundation. We are also grateful for the technical and facility support provided at the Center for High Performance Computing (CHPC) at the University of Utah.

References

1 R. W. Harvey and S. P. Garabedlan, Use of Colloid Filtration Theory in Modeling Movement of Bacteria through a Contaminated Sandy Aquifer, *Environ. Sci. Technol.*, 1991, **25**, 178–185.

2 N. Tufenkji, G. F. Miller, J. N. Ryan, R. W. Harvey and M. Elimelech, Transport of Cryptosporidium oocysts in porous media: Role of straining and physicochemical filtration, *Environ. Sci. Technol.*, 2004, **38**, 5932–5938.

3 L. Liu, Y. Wang, R. Narain and Y. Liu, Functionalized polystyrene microspheres as Cryptosporidium surrogates, *Colloids Surfaces B Biointerfaces*, 2019, **175**, 680–687.

4 J. A. Redman, S. L. Walker and M. Elimelech, Bacterial Adhesion and Transport in Porous Media: Role of the Secondary Energy Minimum, *Environ. Sci. Technol.*, 2004, **38**, 1777–1785.

5 A. B. Cundy, L. Hopkinson and R. L. D. Whitby, Use of iron-based technologies in contaminated land and groundwater remediation: A review, *Sci. Total Environ.*, 2008,

400, 42–51.

6 M. I. Rakowska, D. Kupryianchyk, J. Harmsen, T. Grotenhuis and A. A. Koelmans, In situ remediation of contaminated sediments using carbonaceous materials, *Environ. Toxicol. Chem.*, 2012, **31**, 693–704.

7 C. M. Kocur, D. M. O'Carroll and B. E. Sleep, Impact of nZVI stability on mobility in porous media, *J. Contam. Hydrol.*, 2013, **145**, 17–25.

8 F. Fu, D. D. Dionysiou and H. Liu, The use of zero-valent iron for groundwater remediation and wastewater treatment: A review, *J. Hazard. Mater.*, 2014, **267**, 194–205.

9 B. Song, G. Zeng, J. Gong, J. Liang, P. Xu, Z. Liu, Y. Zhang, C. Zhang, M. Cheng, Y. Liu, S. Ye, H. Yi and X. Ren, Evaluation methods for assessing effectiveness of in situ remediation of soil and sediment contaminated with organic pollutants and heavy metals, *Environ. Int.*, 2017, **105**, 43–55.

10 C. A. Ron, M. Dong, K. L. Wooley and W. P. Johnson, Theory-Guided Targeted Delivery of Nanoparticles in Advective Environmental Porous Media, *Environ. Sci. Technol. Lett.*, 2019, **6**, 617–623.

11 S. Zhu, T. Qu, M. K. Irshad and J. Shang, Simultaneous removal of Cd(II) and As(III) from co-contaminated aqueous solution by α-FeOOH modified biochar, *Biochar*, 2020, **2**, 81–92.

12 R. Rajagopalan and C. Tien, Trajectory analysis of deep-bed filtration with the sphere-in-cell porous media model, *AIChE J.*, 1976, **22**, 523–533.

13 K. Yao, M. T. Habibian and C. R. O'Melia, Water and Waste Water Filtration: Concepts and Applications, *Environ. Sci. Technol.*, 1971, **5**, 1105–1112.

14 J. N. Israelachvili, *Intermolecular and Surface Forces*, Academic Press, Burlington, MA, USA, 3rd ed., 2011.

15 B. Derjaguin and L. Landau, Theory of the stability of strongly charged lyophobic sols and

of the adhesion of strongly charged particles in solutions of electrolytes, *Prog. Surf. Sci.*, 1941, **43**, 30–59.

16 E. J. W. Verwey and J. T. G. Overbeek, Theory of the stability of lyophobic colloids, *J. Phys. Chem.*, 1947, **51**, 631–636.

17 M. Elimelech and C. R. O'Melia, Kinetics of Deposition of Colloidal Particles in Porous Media, *Environ. Sci. Technol.*, 1990, **24**, 1528–1536.

18 S. Bhattacharjee, J. Y. Chen and M. Elimelech, DLVO interaction energy between spheroidal particles and a flat surface, *Colloids Surfaces A Physicochem. Eng. Asp.*, 2000, **165**, 143–156.

19 R. Duffadar and J. M. Davis, Interaction of micrometer-scale particles with nanotextured surfaces in shear flow, *J. Colloid Interface Sci.*, 2007, **308**, 20–29.

20 M. Bendersky and J. M. Davis, DLVO interaction of colloidal particles with topographically and chemically heterogeneous surfaces, *J. Colloid Interface Sci.*, 2011, **353**, 87–97.

21 J. Drelich and Y. U. Wang, Charge heterogeneity of surfaces: Mapping and effects on surface forces, *Adv. Colloid Interface Sci.*, 2011, **165**, 91–101.

22 E. Pazmino, J. Trauscht, B. Dame and W. P. Johnson, Power Law Size-Distributed Heterogeneity Explains Colloid Retention on Soda Lime Glass in the Presence of Energy Barriers, *Langmuir*, 2014, **30**, 5412–5421.

23 J. Trauscht, E. Pazmino and W. P. Johnson, Prediction of Nanoparticle and Colloid Attachment on Unfavorable Mineral Surfaces Using Representative Discrete Heterogeneity, *Langmuir*, 2015, **31**, 9366–9378.

24 X. Li, T. D. Scheibe and W. P. Johnson, Apparent Decreases in Colloid Deposition Rate Coefficients with Distance of Transport under Unfavorable Deposition Conditions: A General Phenomenon, *Environ. Sci. Technol.*, 2004, **38**, 5616–5625.

25 W. P. Johnson and M. Hilpert, Upscaling colloid transport and retention under unfavorable conditions: Linking mass transfer to pore and grain topology, *Water Resour.*

Res., 2013, **49**, 5328–5341.

26 J. F. Schijven, W. Hoogenboezem, S. M. Hassanizadeh and J. H. Peters, Modeling removal of bacteriophages MS2 and PRD1 by dune recharge at Castricum, Netherlands, *Water Resour. Res.*, 1999, **35**, 1101–1111.

27 J. F. Schijven, G. Medema, A. J. Vogelaar and S. M. Hassanizadeh, Removal of microorganisms by deep well injection, *J. Contam. Hydrol.*, 2000, **44**, 301–327.

28 P. Johnson, P. Zhang, M. E. Fuller, T. D. Scheibe, B. J. Mailloux, T. C. Onstott, M. F. DeFlaun, S. S. Hubbard, J. Radtke, W. P. Kovacik and W. Holben, Ferrographic Tracking of Bacterial Transport in the Field at the Narrow Channel Focus Area, Oyster, VA, *Environ. Sci. Technol.*, 2001, **35**, 182–191.

29 P. Zhang, W. P. Johnson, T. D. Scheibe, K. Choi, F. C. Dobbs and B. J. Mailloux, Extended tailing of bacteria following breakthrough at the Narrow Channel Focus Area, Oyster, Virginia, *Water Resour. Res.*, 2001, **37**, 2687–2698.

30 W. P. Johnson, A. Rasmuson, C. Ron, B. Erickson, K. VanNess, D. Bolster and B. Peters, Anionic nanoparticle and microplastic non-exponential distributions from source scale with grain size in environmental granular media, *Water Res.*, 2020, **182**, 116012.

31 A. Rasmuson, B. Erickson, M. Borchardt, M. Muldoon and W. P. Johnson, Pathogen Prevalence in Fractured versus Granular Aquifers and the Role of Forward Flow Stagnation Zones on Pore-Scale Delivery to Surfaces, *Environ. Sci. Technol.*, 2019, **54**, 137–145.

32 N. Tufenkji and M. Elimelech, Deviation from the Classical Colloid Filtration Theory in the Presence of Repulsive DLVO Interactions, *Langmuir*, 2004, **20**, 10818–10828.

33 X. Li and W. P. Johnson, Nonmonotonic variations in deposition rate coefficients of microspheres in porous media under unfavorable deposition conditions, *Environ. Sci. Technol.*, 2005, **39**, 1658–1665.

34 W. P. Johnson, Quantitative Linking of Nanoscale Interactions to Continuum-Scale

Nanoparticle and Microplastic Transport in Environmental Granular Media, *Environ. Sci. Technol.*, 2020, **54**, 8032–8042.

35 W. P. Johnson, A. Rasmuson, E. Pazmiño and M. Hilpert, Why Variant Colloid Transport Behaviors Emerge among Identical Individuals in Porous Media When Colloid–Surface Repulsion Exists, *Environ. Sci. Technol.*, 2018, **52**, 7230–7239.

36 L. K. Koopal and W. H. van Riemsdijk, Electrosorption on random and patchwise heterogeneous surfaces: electrical double-layer effects, *J. Colloid Interface Sci.*, 1989, **128**, 188–200.

37 L. Song, P. R. Johnson and M. Elimelech, Kinetics of Colloid Deposition onto Heterogeneously Charged Surfaces in Porous Media, *Environ. Sci. Technol.*, 1994, **28**, 1164–1171.

38 R. D. Duffadar and J. M. Davis, Dynamic adhesion behavior of micrometer-scale particles flowing over patchy surfaces with nanoscale electrostatic heterogeneity, *J. Colloid Interface Sci.*, 2008, **326**, 18–27.

39 R. Duffadar, S. Kalasin, J. M. Davis and M. M. Santore, The impact of nanoscale chemical features on micron-scale adhesion: Crossover from heterogeneity-dominated to mean-field behavior, *J. Colloid Interface Sci.*, 2009, **337**, 396–407.

40 A. Rasmuson, K. VanNess, C. A. Ron and W. P. Johnson, Hydrodynamic versus Surface Interaction Impacts of Roughness in Closing the Gap between Favorable and Unfavorable Colloid Transport Conditions, *Environ. Sci. Technol.*, 2019, **53**, 2450–2459.

41 C. A. Ron, K. VanNess, A. Rasmuson and W. P. Johnson, How nanoscale surface heterogeneity impacts transport of nano- to micro-particles on surfaces under unfavorable attachment conditions, *Environ. Sci. Nano*, 2019, **6**, 1921–1931.

42 L. S. Dorobantu, S. Bhattacharjee, J. M. Foght and M. R. Gray, Atomic Force Microscopy Measurement of Heterogeneity in Bacterial Surface Hydrophobicity, *Langmuir*, 2008, **24**, 4944–4951.

43 K. Shellenberger and B. E. Logan, Effect of molecular scale roughness of glass beads on colloidal and bacterial deposition, *Environ. Sci. Technol.*, 2002, **36**, 184–189.

44 P. Taboada-Serrano, V. Vithayaveroj, S. Yiacoumi and C. Tsouris, Surface charge heterogeneities measured by atomic force microscopy, *Environ. Sci. Technol.*, 2005, **39**, 6352–6360.

45 S. Kalasin and M. M. Santore, Hydrodynamic crossover in dynamic microparticle adhesion on surfaces of controlled nanoscale heterogeneity, *Langmuir*, 2008, **24**, 4435–4438.

46 M. K. Shave, S. Kalasin, E. Ying and M. M. Santore, Nanoscale Functionalized Particles with Rotation-Controlled Capture in Shear Flow, *ACS Appl. Mater. Interfaces*, 2018, **10**, 29058–29068.

47 H. Ma, C. Bolster, W. P. Johnson, K. Li, E. Pazmino, K. M. Camacho, A. C. Anselmo and S. Mitragotri, Coupled influences of particle shape, surface property and flow hydrodynamics on rod-shaped colloid transport in porous media, *J. Colloid Interface Sci.*, 2020, **577**, 471–480.

48 K. Li and H. Ma, Rotation and Retention Dynamics of Rod-Shaped Colloids with Surface Charge Heterogeneity in Sphere-in-Cell Porous Media Model, *Langmuir*, 2019, **35**, 5471–5483.

49 S. A. Bradford, H. Kim, C. Shen, S. Sasidharan and J. Shang, Contributions of Nanoscale Roughness to Anomalous Colloid Retention and Stability Behavior, *Langmuir*, 2017, **33**, 10094–10105.

50 A. Rasmuson, E. Pazmino, S. Assemi and W. P. Johnson, Contribution of Nano- to Microscale Roughness to Heterogeneity: Closing the Gap between Unfavorable and Favorable Colloid Attachment Conditions, *Environ. Sci. Technol.*, 2017, **51**, 2151–2160.

51 H. Ohshima, Electrophoresis of soft particles: Analytic approximations, *Electrophoresis*, 2006, **27**, 526–533.

52 W. Kern and D. A. Puotinen, Interview with W. Kern, *RCA Rev.*, 1970, **31**, 187–206.

53 M. Tong and W. P. Johnson, Excess colloid retention in porous media as a function of colloid size, fluid velocity, and grain angularity, *Environ. Sci. Technol.*, 2006, **40**, 7725–7731.

54 B. J. Kirby and E. F. Hasselbrink, Zeta potential of microfluidic substrates: 1. Theory, experimental techniques, and effects on separations, *Electrophoresis*, 2004, **25**, 187–202.

55 C. Tien and A. C. Payatakes, Advances in deep bed filtration, *AIChE J.*, 1979, **25**, 737–759.

56 I. L. Molnar, W. P. Johnson, J. I. Gerhard, C. S. Willson and D. M. O'Carroll, Predicting colloid transport through saturated porous media: A critical review, *Water Resour. Res.*, 2015, **51**, 6804–6845.

57 H. Ma, E. Pazmino and W. P. Johnson, Surface heterogeneity on hemispheres-in-cell model yields all experimentally-observed non-straining colloid retention mechanisms in porous media in the presence of energy barriers, *Langmuir*, 2011, **27**, 14982–14994.

58 K. VanNess, A. Rasmuson, C. A. Ron and W. P. Johnson, A Unified Force and Torque Balance for Colloid Transport: Predicting Attachment and Mobilization under Favorable and Unfavorable Conditions, *Langmuir*, 2019, **35**, 9061–9070.

59 E. M. V. Hoek and G. K. Agarwal, Extended DLVO interactions between spherical particles and rough surfaces, *J. Colloid Interface Sci.*, 2006, **298**, 50–58.

60 S. Torkzaban and S. A. Bradford, Critical role of surface roughness on colloid retention and release in porous media, *Water Res.*, 2016, **88**, 274–284.

61 N. Kozlova and M. M. Santore, Manipulation of Micrometer-Scale Adhesion by Tuning Nanometer-Scale Surface Features, *Langmuir*, 2006, **22**, 1135–1142.

62 T. Li, C. Shen, S. Wu, C. Jin and S. A. Bradford, Synergies of surface roughness and hydration on colloid detachment in saturated porous media: Column and atomic force microscopy studies, *Water Res.*, 2020, **183**, 116068.

63 C. Shen, Y. Jin, J. Zhuang, T. Li and B. Xing, Role and importance of surface heterogeneities in transport of particles in saturated porous media, *Crit. Rev. Environ. Sci.*

Technol., 2019, 1–86.

64 G. Shi, H. V. Atkinson, C. M. Sellars and C. W. Anderson, Application of the Generalized Pareto Distribution to the estimation of the size of the maximum inclusion in clean steels, *Acta Mater.*, 1999, **47**, 1455–1468.

65 D. G. Harlow and R. P. Wei, A probability model for the growth of corrosion pits in aluminum alloys induced by constituent particles, *Eng. Fract. Mech.*, 1998, **59**, 305–325.

66 J. Buffle and G. G. Leppard, Characterization of Aquatic Colloids and Macromolecules. 1. Structure and Behavior of Colloidal Material, *Environ. Sci. Technol.*, 1995, **29**, 2169–2175.

67 O. Atteia and R. Kozel, Particle size distributions in waters from a karstic aquifer: from particles to colloids, *J. Hydrol.*, 1997, **201**, 102–119.

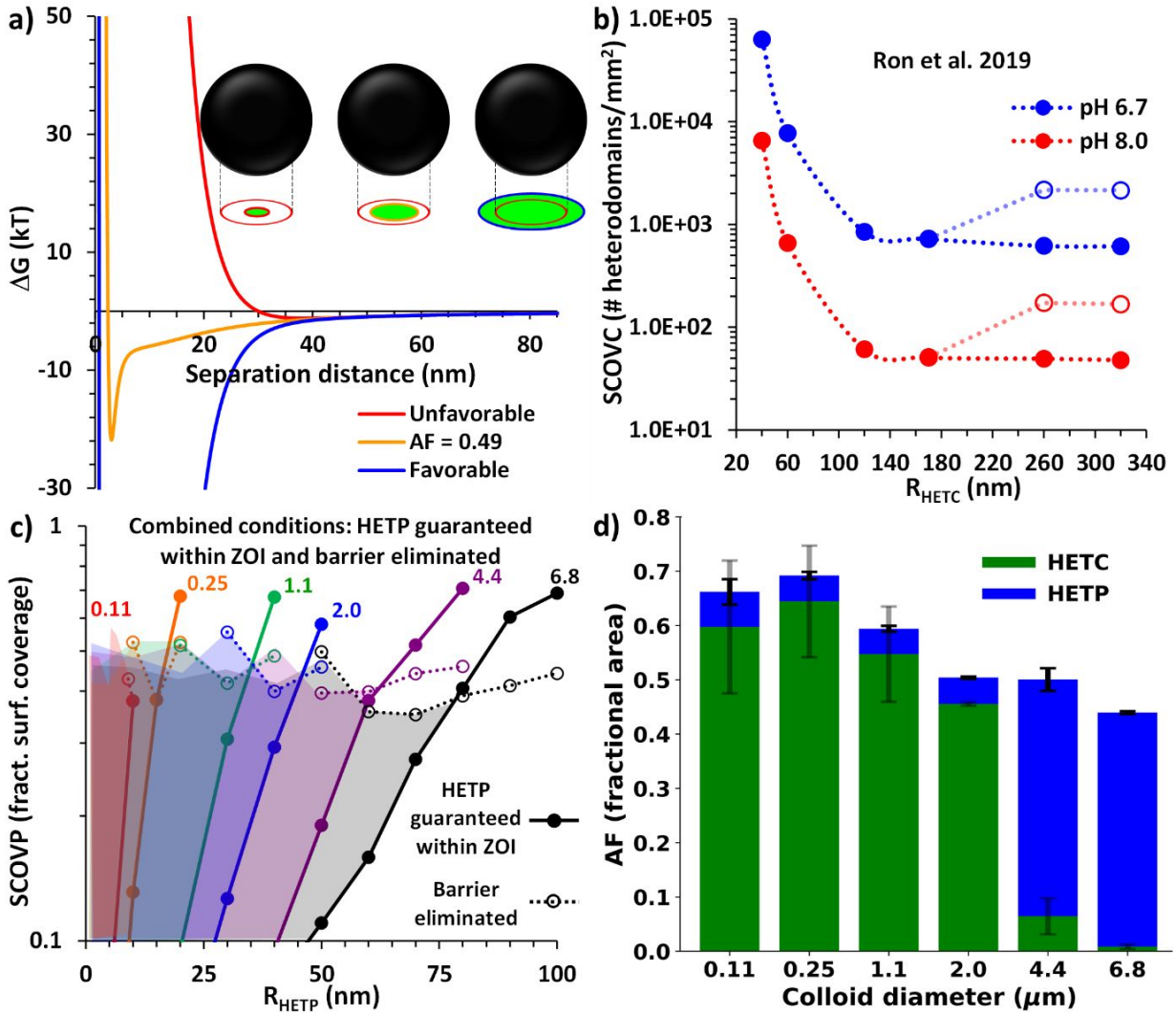

Figure 1. a) Colloid-collector XDLVO energy profiles (ΔG) for 1.1 μm CML. Projected red circumference represents the colloid-collector ZOI, and colored circles represent heterodomains of sizes small (red), medium (gold), and large (blue) relative to the ZOI, with the same colors for the corresponding energy profiles. **b)** Closed circles correspond to distribution of surface coverage (SCOVC) versus radius (R_{HETC}) of heterodomains on the collector as used in Ron et al.[41] Open circles correspond to SCOVC required to explain experimentally-observed η for > 2.0 μm colloids. **c)** Surface coverage (SCOVP) as a function of radius (R_{HETP}) of heterodomains on the colloid (HETP) that: i) guarantees that at least one HETP will be completely encompassed by the ZOI regardless of colloid orientation (rotation) (solid lines); and ii) eliminates the repulsive barrier solely by HETP (HETC absent) (dotted lines). Shaded areas represent SCOVP and R_{HETP} space within which transport simulations were performed without

explicit colloid rotation. Number labels designate corresponding colloid diameter in μm (6.0 mM IS and pH 8.0). For separate conditions see Figure SI-2a and b. **d)** Contribution of HETC and HETP to the fraction of the ZOI area (AF) that eliminates the repulsive barrier and yields colloid attachment in mechanistic trajectory simulations under 6.0 mM IS and pH 8.0. Error bars denote maximum and minimum contributions to AF for attached CML in mechanistic trajectory simulations.

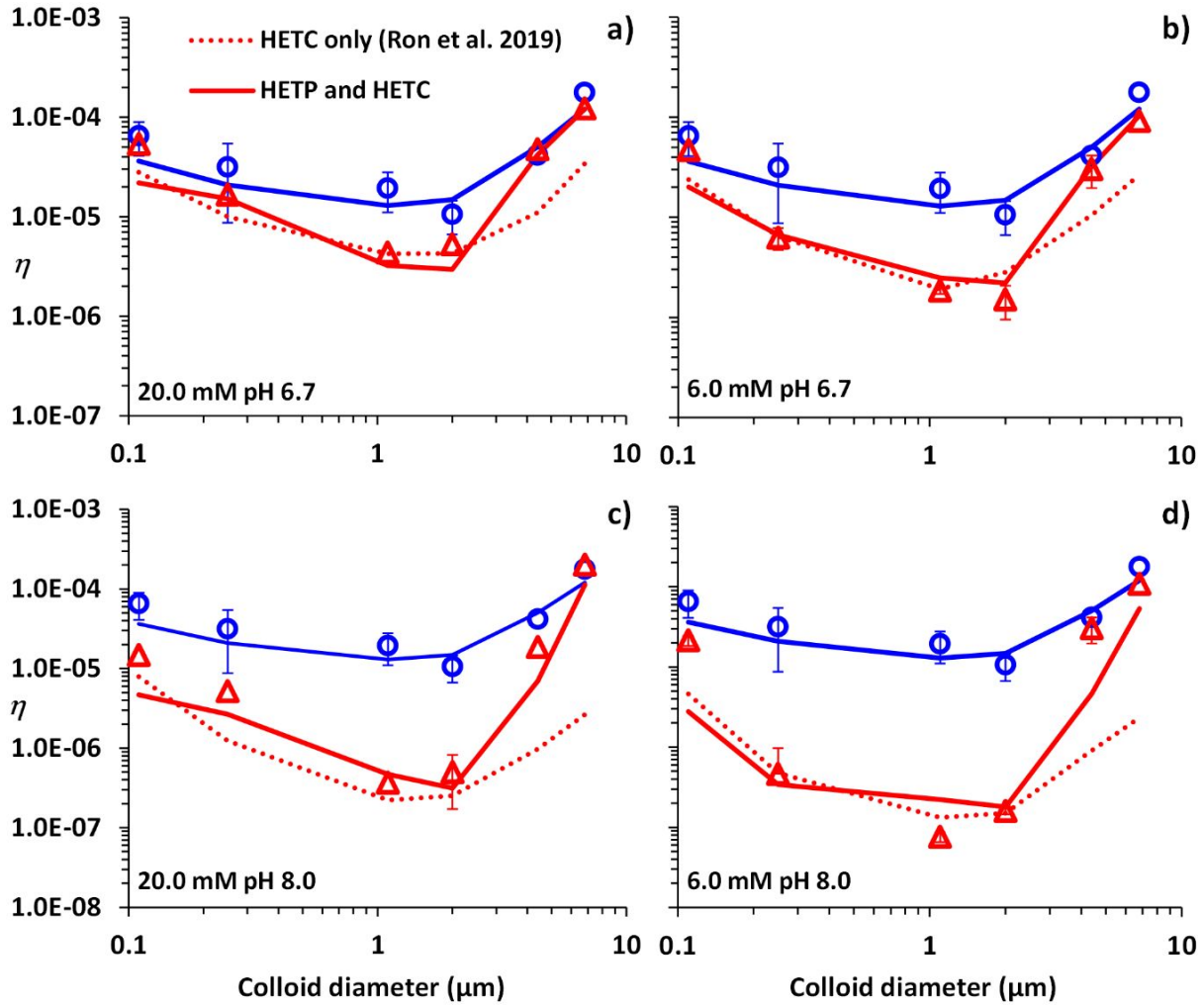

Figure 2. Experimentally-observed collector efficiencies (η) for CML-water-glass system at indicated IS and pH values in an impinging jet system with v_{jet} = 1.7E-3 ms^{-1}.[41] Blue circles and red triangles correspond to favorable and unfavorable experimental conditions, respectively. Error bars denote maximum and minimum values for replicate experiments. Solid lines represent simulation results under favorable conditions (blue) and unfavorable conditions (red), with DRNH either solely on the collector (HETC) (red dotted lines) as described in Ron et al.,[41] or on both the collector and colloid (HETP) (red solid lines) as described herein.

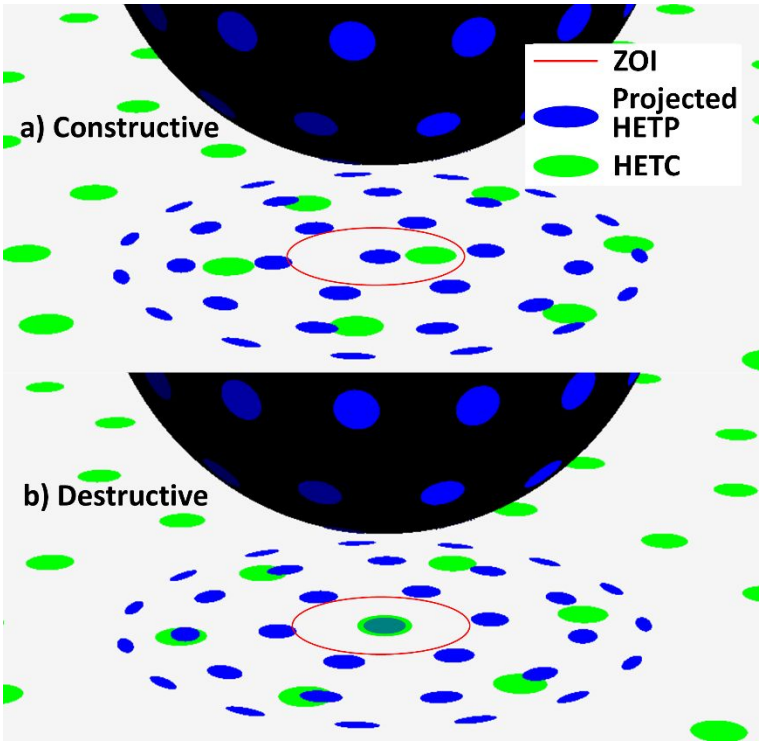

Figure 3. a) Representation of constructive (attractive) contribution from HETC and projected HETP to colloid-collector interactions. **b)** Representation of destructive (repulsive) contribution from HETC and projected HETP to colloid-collector interactions. In this study we only considered contributions to from HETC and HETP that were partially or fully encompassed by the zone of interaction (ZOI).

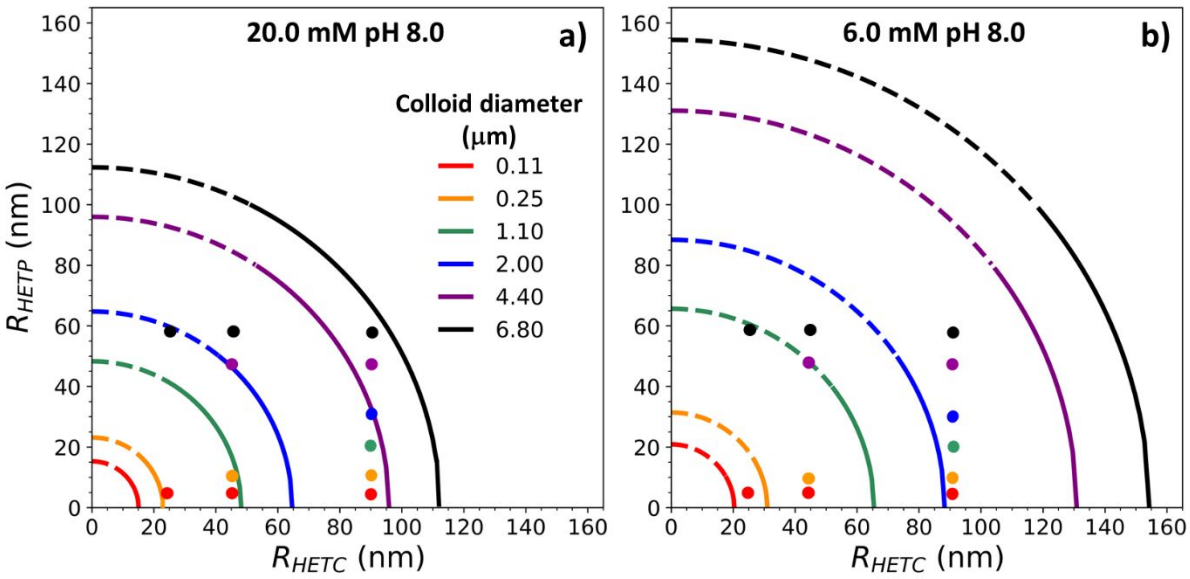

Figure 4. Quadratic relationship (quarter-circle lines) of required heterodomain radii on collector (R_{HETC}) and colloid (R_{HETP}) surfaces that together (complimentarily) eliminate the repulsive barrier (Equation 1). The relationship assumes that the projection of HETP exists fully within the ZOI without overlapping HETC, such that their contributions to AF are solely constructive. The dashed portion of the quarter circle lines indicate the threshold R_{HETP} above which HETP are too few in number to guarantee that one HETP will lie within the ZOI regardless of colloid orientation. Closed circles correspond to combinations of R_{HETC} and R_{HETP} active in attachment in colloid trajectory simulations, with color corresponding to colloid size in legend.

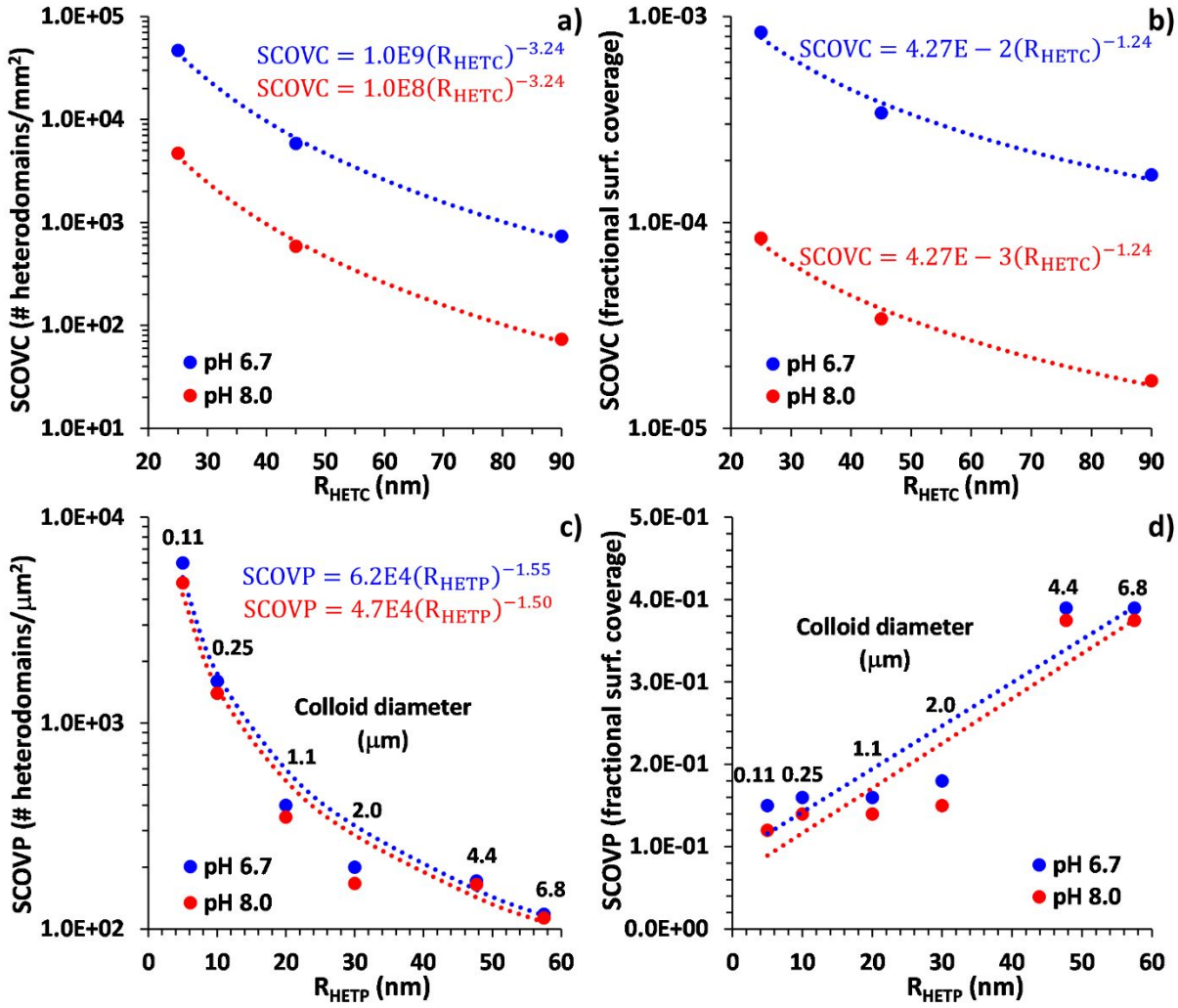

Figure 5. DRNH distributions utilized in colloid trajectory simulations, with surface coverage (SCOVC) as a function of radius (R_{HETC}) of heterodomains on the collector (top row, a and b), with surface coverage (SCOVP) as a function of radius (R_{HETP}) of heterodomains on the colloid (bottom row, c and d), each expressed as number per area (left column, a and c) and fraction of total surface area (right column, b & d). Equations correspond to fitted power law distributions (dotted lines). The distributions applied for both IS (6.0 and 20.0 mM) studied.

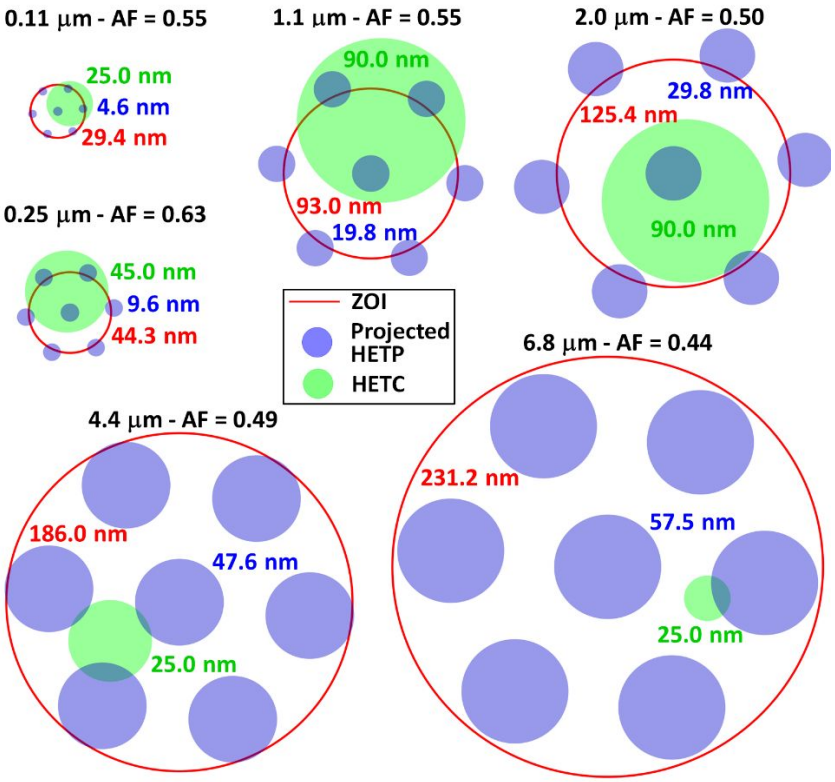

Figure 6. Representative attachment outcomes regarding constructive (no heterodomain overlap) and destructive (heterodomain overlap) contributions from HETC (green) and projected HETP (blue) within ZOI (red) as obtained from mechanistic trajectory simulations under 6.0 mM IS and pH 8.0 condition. These outcomes correspond to simulations and parameters shown in Figures 1d, 2d, 3b and 5.

Abstract Art